Supporting Information

Covalent modification of franckeite with maleimides: connecting molecules and van der Waals heterostructures

Julia Villalva,† Sara Moreno-Da Silva,† Palmira Villa,‡ Luisa Ruiz-González,§ Cristina Navío,† Saül García-Orrit, † Víctor Vega-Mayoral, † Juan Cabanillas-González, † Andrés Castellanos-Gómez,⬩ Emerson Giovanelli,† and Emilio M. Pérez*†

†   IMDEA Nanociencia; c/ Faraday 9, Campus de Cantoblanco; 28049 Madrid, Spain.
‡   Instituto Pluridisciplinar; Universidad Complutense de Madrid; Paseo de Juan XXIII Nº 1, 28040 Madrid, Spain.
§   Departamento de Química Inorgánica; Facultad de ciencias químicas, Universidad Complutense de Madrid, Av. Complutense s/n, 28040 Madrid, Spain.
⬩   Instituto de Ciencia de Materiales de Madrid (ICMM-CSIC), Sor Juana Inés de la Cruz, 3, Campus de Cantoblanco, 28049 Madrid, Spain.

INDEX

S1. Materials and methods

a. Chemicals and reagents

The bulk franckeite mineral was obtained from mine San José, Oruro (Bolivia). The same crystal was used for all experiments. All general reagents were obtained from usual commercial sources and used without further purification. The *N*-benzyl maleimide was purchased from TCI. Flash chromatography was performed using silica gel (Merck, Kieselgel 60, 230-240 mesh, or Scharlau 60, 230-240 mesh).

b. Equipment

NMR

NMR spectra were recorded on a BrukerAvance 400 (^{1}H: 400 MHz, ^{13}C: 101 MHz) at 298 K using the solvent noted in each case. Coupling constants (*J*) are denoted in Hz and chemical shifts (δ) in ppm. Multiplicities are denoted as follows: s = singlet, d = doublet, t = triplet, m = multiplet, b = broad.

^{1}H high-resolution magic angle spinning (HRMAS) NMR spectroscopy (^{1}H-HR-MAS-NMR) experiments were performed on a vertical magnet Bruker AV500 operating at 500 MHz. The samples were introduced as solids in ZrO_2 rotors with 12 µL internal volume and a drop of D_2O was added. Standard solvent suppressed spectra (NOESYPRESAT) were acquired into 32 k data points, averaged over 512 acquisitions. The total acquisition time was ~26 min, with a spectral width of 8012 Hz. All spectra were processed using TOPSPIN software.

UV/Vis spectroscopy

The extinction spectra were measured in a quartz cuvette (path length = 1 cm) with a Cary 5000 UV/Vis/NIR spectrophotometer.

Raman spectroscopy

The colloidal samples were drop-cast and dried onto glass slides at 50 ºC. Their Raman spectra were recorded with a Bruker Senterra confocal Raman microscope (Bruker Optic, Ettlingen, Germany, resolution 3-5 cm^{-1}) using the following parameters: objective NA 0.75, 50V; laser excitation: 633 nm, 0.2 mW.

Fourier-transform infrared spectroscopy with attenuated total reflection (FT-ATR-IR)

Infrared spectra with attenuated total reflection (ATR-IR) were performed with a Bruker ALPHA FT-IR spectrometer.

XPS Spectroscopy

XPS (X-ray Photoelectron Spectroscopy) measurements were performed under Ultra High Vacuum conditions (UHV, with a base pressure of 5·10^{-10} mbar), using a monochromatic Al Kα line as exciting photon source for core level analysis (hν = 1486.7 eV). The emitted photoelectrons were collected in a hemispherical energy analyzer (SPHERA-U7, pass energy set to 20 eV for the XPS measurements to have a resolution of 0.6 eV) and to compensate the built up charge on the sample surface it was necessary the use of a Flood Gun (FG-500, Specs), with low energy electrons of 3 eV and 40 µA.

Photoluminescence excitation (PLE)

Photoluminescence excitation intensity maps (PLE) were obtained with a FluoroLog 3 spectrometer from HORIBA Yobin Yvon using a 450 W Xenon lamp and a Symphony InGaAs

array in combination with an iHR320 imaging spectrometer. For the visible range, a Fluoromax3 spectrometer from HORIBA Yobin Yvon was used.

Atomic Force Microscopy

AFM images were acquired using a JPK NanoWizard II AFM working in dynamic mode. NT-MDT NSG01 silicon cantilevers, with typical values of 5.1 N·m^{-1} spring constant and 150 kHz resonant frequency, were employed under ambient conditions in air.

Transmission Electron Microscopy

Transmission electron microscopy (TEM) images were obtained with a JEOL-JEM 2100F (2.5 Å resolution) instrument operating at 200 kV. The samples were prepared by dropcasting the colloidal franckeite samples onto 200 square mesh covered by holey carbon.

Thermogravimetric Analysis

Thermogravimetric analyses (TGA) were performed using a TA Instruments TGAQ500 with a ramp of 10 °C/min under N_2 from 100 to 1000 °C.

Transient absorption spectroscopy

TAS measurements were carried out using a femtosecond Clark-MXR CPA210 regenerative amplifier as a primary laser pulses source. With an initial 120 fs long pulses centered at 775 nm and with 1 KHz repetition rate. The laser output is split between pump and probe beam. Pump beam is focused in a SHG BBO crystal, generating blue light (387.5 nm) before it is focused on the sample. Probe beam is focused on a CaF_2 glass to generate a white light supercontinuum and overlapped with the pump on the sample. The transmitted probe beam was sent to a prism spectrometer (Entwicklungsburo Stressing) and detected with a linear CCD array (VIS-Enhanced InGaAs Hamamatsu Photonics). A software synchronizes the delay line with the acquisition system and records spectra at single shot. Measurements were performed with pump and probe beams polarized at magic angle.

Time-resolved photoluminescence

Time-resolved photoluminescence measurements were performed with a HydraHarp multichannel time correlator single photon counting unit from Picoquant GmbH. Excitation at 405 nm was provided by a Picoquant Sepia picosecond diode laser delivering pulses of 80 ps a 2.5 MHz repetition rate. Single wavelength detection was conducted with a thermo-electrically cooled PMA Hybrid 50 photomultiplier assembly from Picoquant coupled to a 0.5 m length SP-2558 Princeton Instruments (Acton Research) spectrometer equipped with a 600 lines/mm grating.

S2. TPP-maleimide synthesis

a)
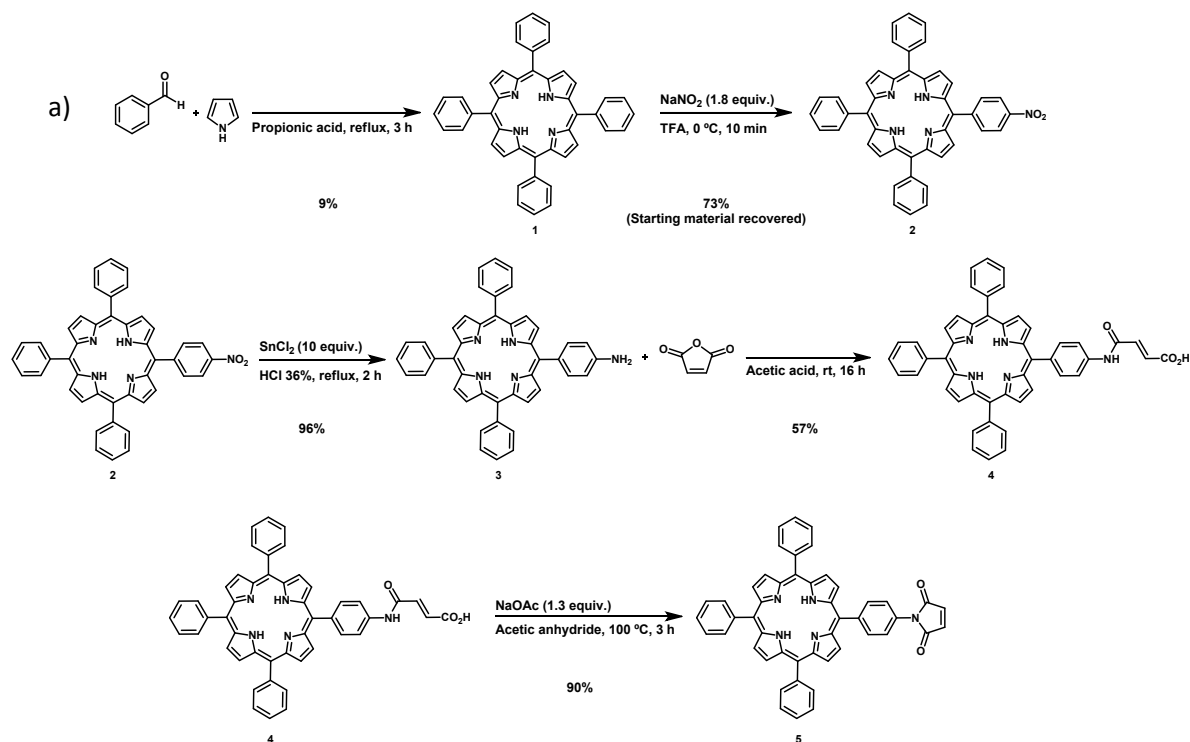
Meso-tetraphenylporphyrin (1).[1] Pyrrole (8.70 g, 0.13 mmol, 1.00 equiv.) and benzaldehyde (12.0 mL, 0.12 mmol, 1.00 equiv.) were stirred under reflux in propionic acid (300 mL) for 3 h. After this time the reaction was cooled to room temperature, washed with hot methanol and dried under vacuum to afford the pure product as a purple solid; yield: 1.90 g (9%). **^{1}H NMR (400 MHz, CDCl$_3$)** δ (ppm): 8.85 (s, 8H), 8.22 (d, J = 6.1 Hz, 8H), 7.80 – 7.73 (m, 12H), -2.77 (s, 2H).
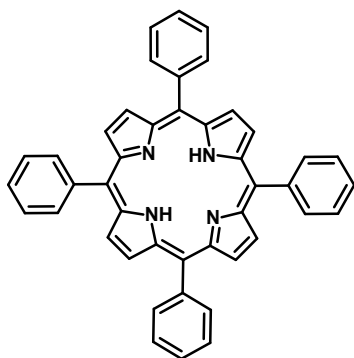
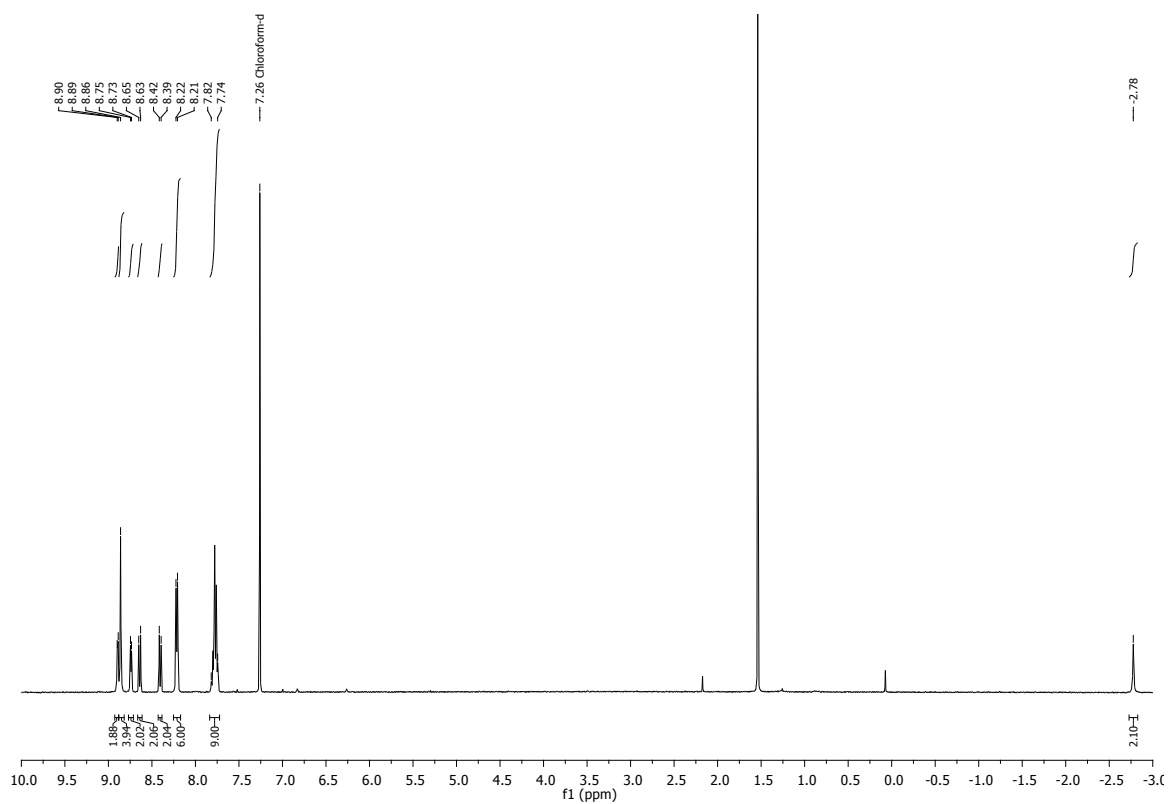**¹H NMR (400 MHz, CDCl₃)**
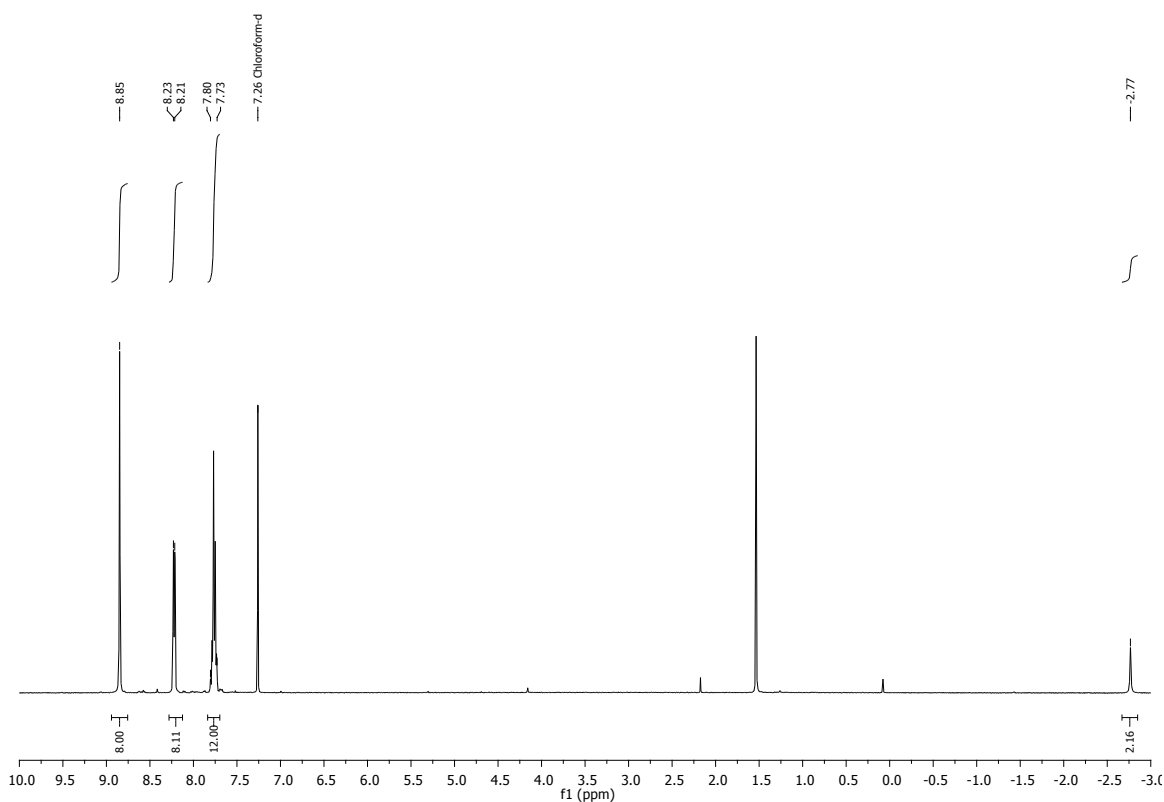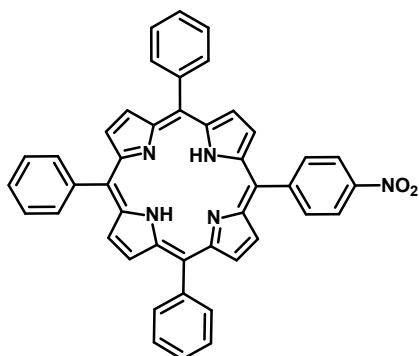
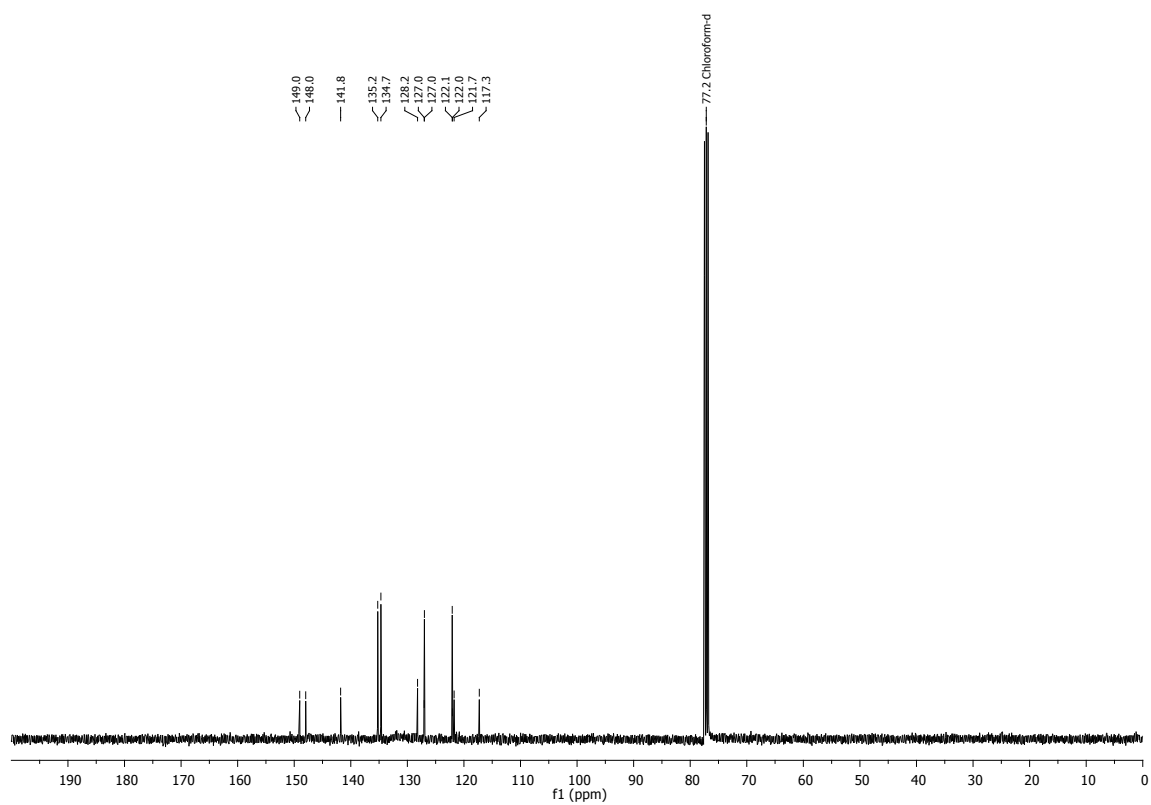**5-(4'-nitrophenyl)-10,15,20-triphenylporphyrin (2).[2]** Meso-tetraphenylporphyrin (1) (3.69 g, 6.00 mmol, 1.00 equiv.) was dissolved in trifluoroacetic acid (55 mL). Sodium nitrite (0.75 g, 10.8 mmol, 1.80 equiv.) was added. The mixture was stirred for 10 min at 0 °C. The resulting solution was transferred to an Erlenmeyer containing a 1:1 chloroform/water mixture. The trifluoroacetic acid was neutralized with saturated aqueous NaHCO₃. The mixture was washed three times with water, dried over magnesium sulfate and the solvent was evaporated under reduced pressure. The residue was purified by silica gel chromatography using CH_2Cl_2/hexane (6:4) as eluent to afford the final product as a purple solid; yield: 2.74 g (73%). **¹H NMR (400 MHz, CDCl₃)** δ (ppm): 8.89 (d, J = 4.8 Hz, 2H), 8.86 (s, 4H), 8.74 (d, J = 4.7 Hz, 2H), 8.64 (d, J = 8.5 Hz, 2H), 8.40 (d, J = 8.5 Hz, 2H), 8.22 – 8.21 (m, 6H), 7.82 – 7.74 (m, 9H), -2.78 (s, 2H). **¹³C NMR (101 MHz, CDCl₃)** δ (ppm): 149.0, 148.0, 141.8, 135.2, 134.7, 128.2, 127.0, 127.0, 122.1, 122.0, 121.7, 117.3.
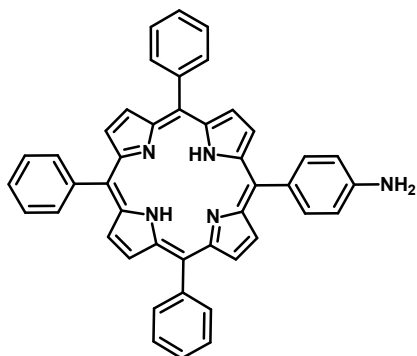
^{1}H NMR (400 MHz, CDCl$_3$)

8.90
8.89
8.86
8.75
8.73
8.65
8.63
8.42
8.39
8.22
8.21
7.82
7.74
7.26 Chloroform-d
−2.78

1.88
3.94
2.02
2.06
2.04
6.00
9.00
2.10

10.0 9.5 9.0 8.5 8.0 7.5 7.0 6.5 6.0 5.5 5.0 4.5 4.0 3.5 3.0 2.5 2.0 1.5 1.0 0.5 0.0 -0.5 -1.0 -1.5 -2.0 -2.5 -3.0
f1 (ppm)

^{13}C NMR (101 MHz, CDCl$_3$)

149.0
148.0
141.8
135.2
134.7
128.2
127.0
122.1
122.0
121.7
117.3
77.2 Chloroform-d

190 180 170 160 150 140 130 120 110 100 90 80 70 60 50 40 30 20 10 0
f1 (ppm)

6

5-(4'-aminophenyl)-10,15,20-triphenylporphyrin (3).[3] A mixture of 5-(4'-nitrophenyl)-10,15,20-triphenylporphyrin (2) (2.74 g, 4.15 mmol, 1.00 equiv.) and tin chloride (9.40 g, 41.5 mmol, 10.0 equiv.) was refluxed in HCl 36% (300 mL) for 2 h. After this time, it was cooled to room temperature, filtered and washed with H_2O several times. Recrystallization from petroleum ether-ethyl acetate afforded the final product as a purple solid; yield: 2.50 g (96%). **^{1}H NMR (400 MHz, CDCl$_3$)** δ (ppm): 1H NMR (400 MHz, CDCl3) δ 8.94 (d, *J* = 4.7 Hz, 2H), 8.83 (s, 6H), 8.22 (d, *J* = 7.4 Hz, 6H), 8.00 (d, *J* = 8.2 Hz, 2H), 7.80 – 7.71 (m, 9H), 7.07 (d, *J* = 8.2 Hz, 2H), 4.06 (s, 2H), -2.75 (s, 2H). **^{13}C NMR (101 MHz, CDCl$_3$)** δ (ppm): 142.5, 135.9, 134.7, 127.8, 126.8, 120.1, 113.6.
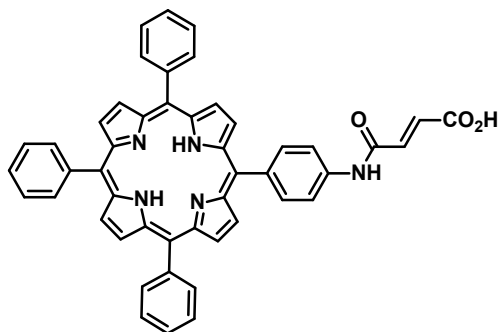
^{1}H NMR (400 MHz, CDCl$_3$)
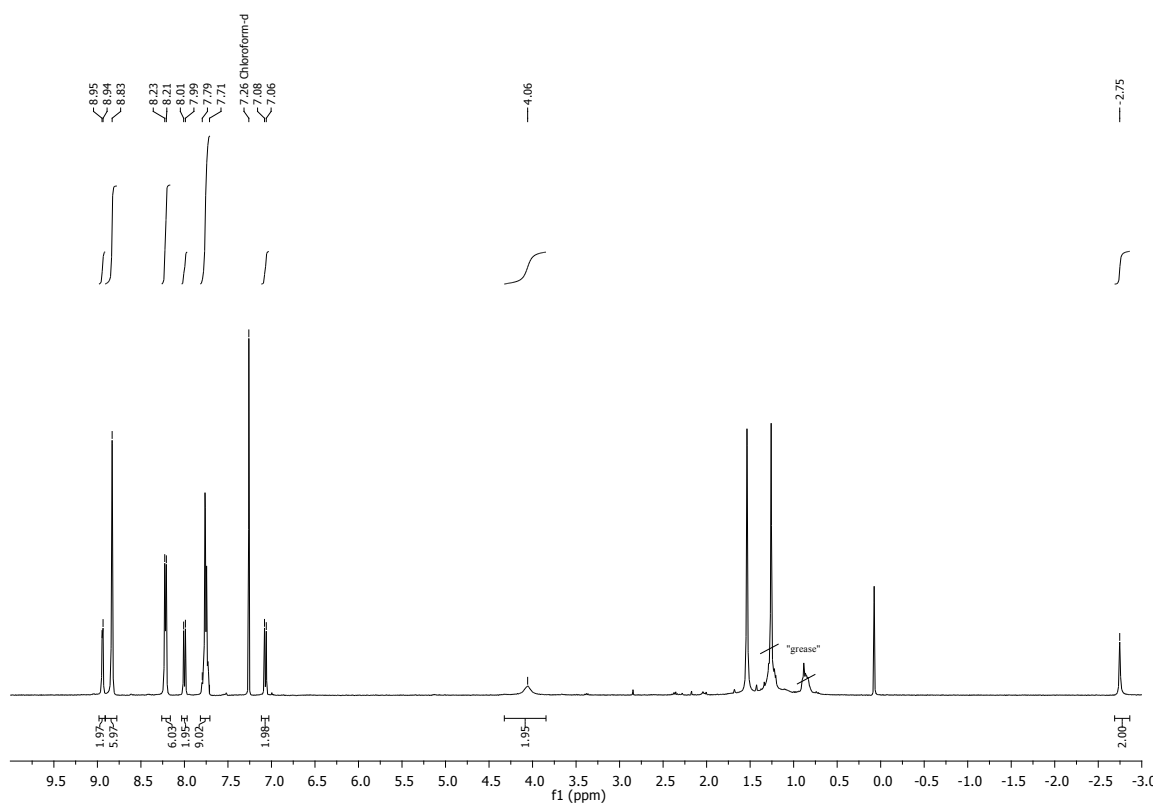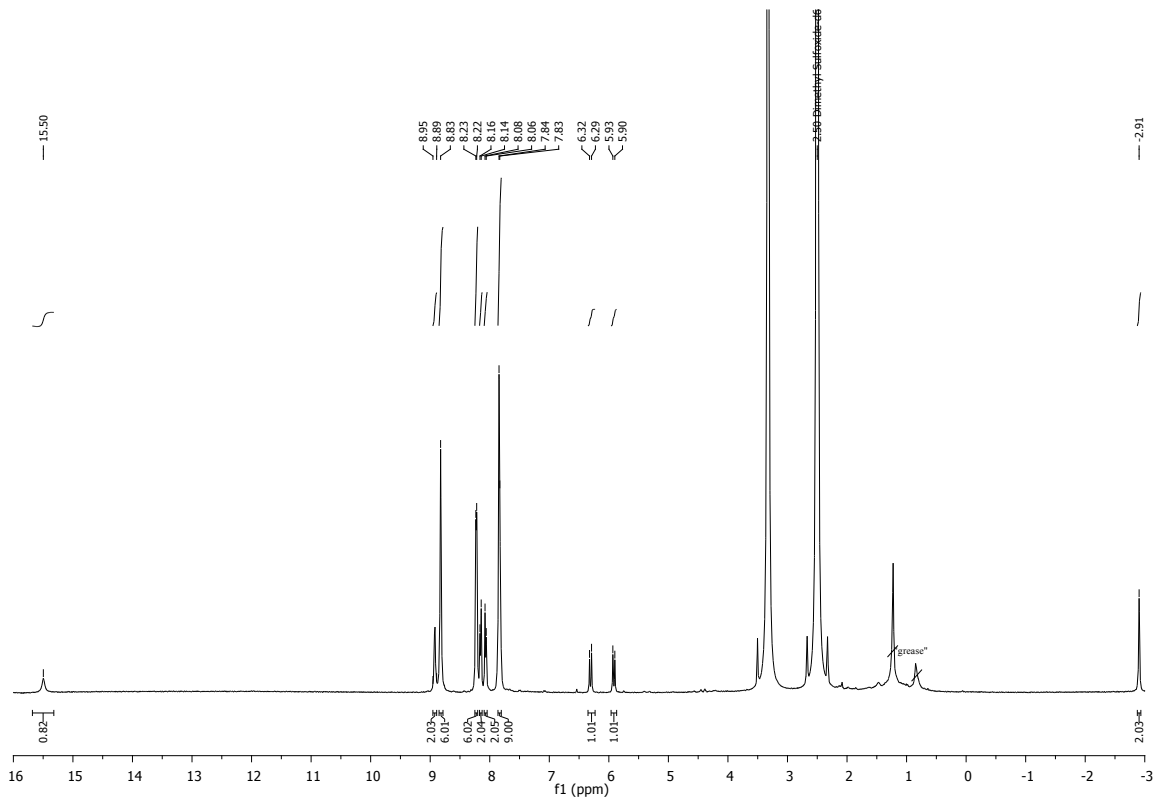

^{13}C NMR (101 MHz, CDCl$_3$)
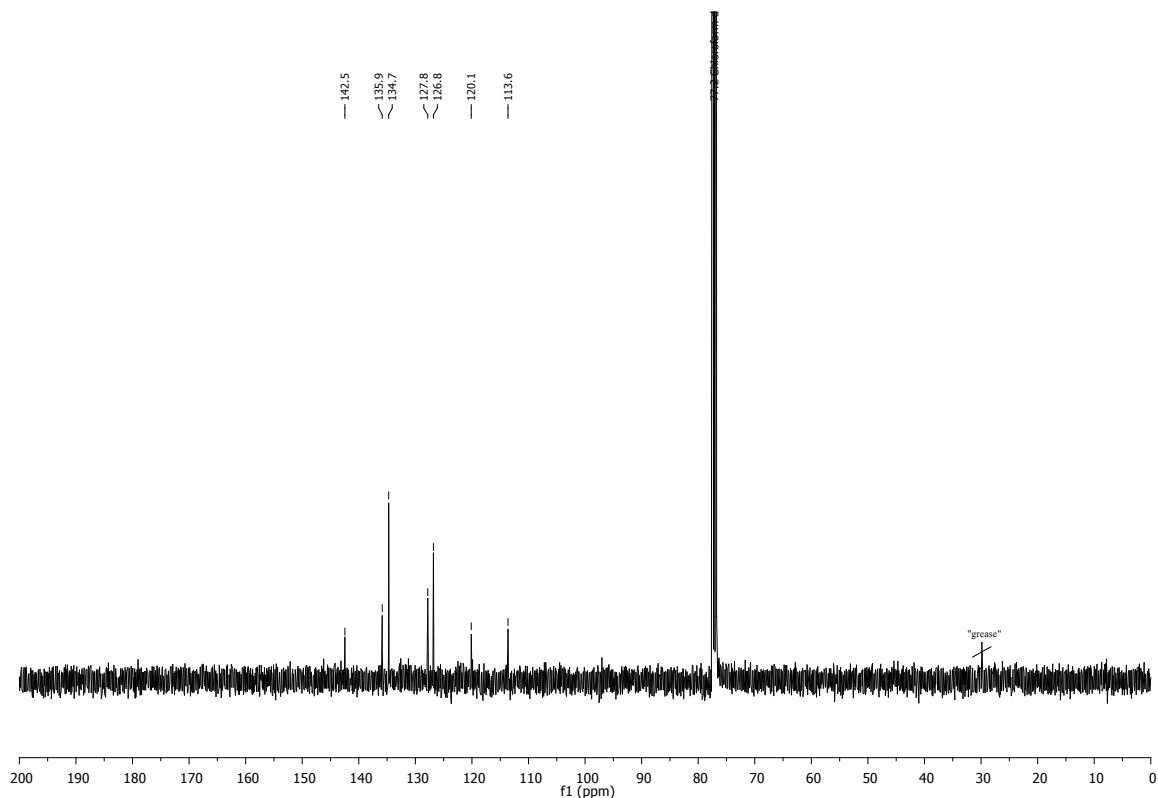
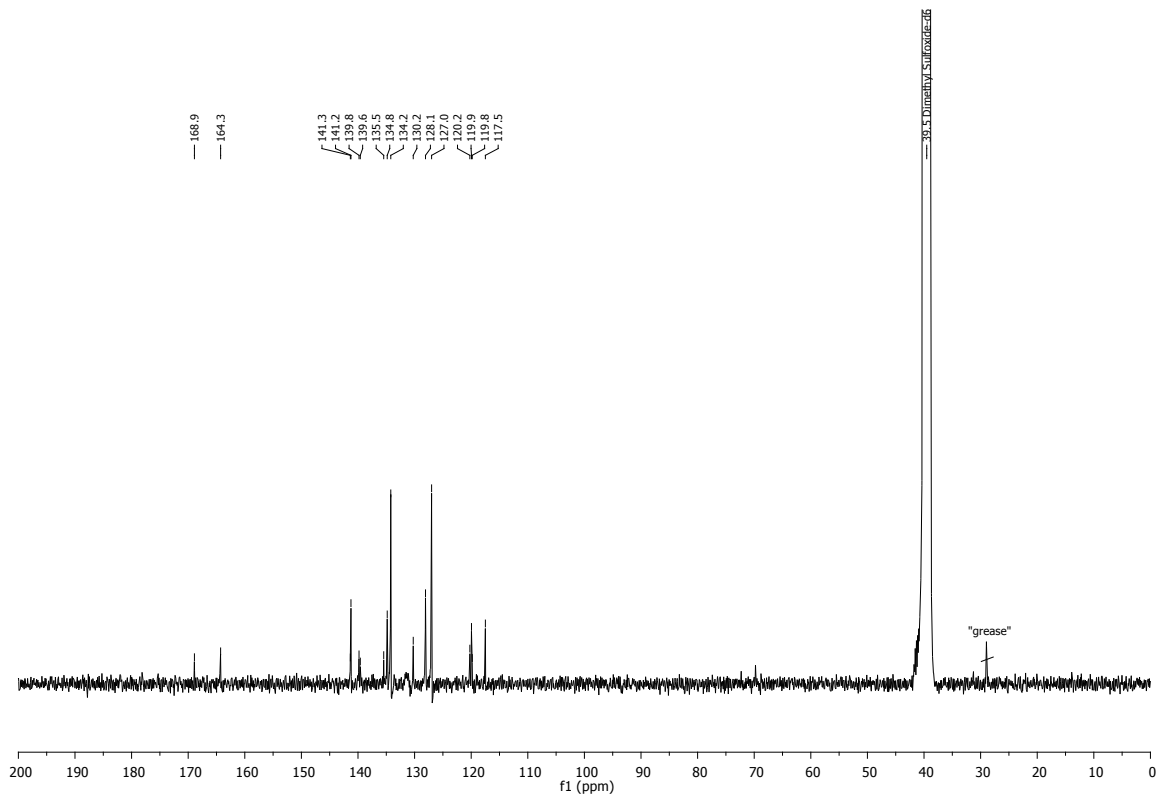**5-[4'-(*N*-Phenylmaleamic acid)]-10,15,20-triphenylporphyrin (4).** A solution of 5-(4'-aminophenyl)-10,15,20-triphenylporphyrin (3) (2.50 g, 3.97 mmol, 1.00 equiv.) and maleic anhydride (0.93 g, 9.53 mmol, 2.40 equiv.) in acetic acid (300 mL) was stirred overnight at room temperature under the absence of moisture. Next day, it was extracted with $CHCl_3$ and washed several times with water. The residue was purified by silica gel chromatography using $CHCl_3$/methanol (6:4) as eluent to afford the final product as a purple solid; yield: 7.65 g (57%). **^{1}H NMR (400 MHz, CDCl$_3$)** δ (ppm): 15.50 (s, 1H), 8.92 (d, *J* = 24.6 Hz, 2H), 8.83 (s, 6H), 8.23 – 8.22 (m, 6H), 8.15 (d, *J* = 8.1 Hz, 2H), 8.07 (d, *J* = 8.1 Hz, 2H), 7.84 – 7.83 (m, 9H), 6.31 (d, *J* = 13.4 Hz, 1H), 5.92 (d, *J* = 13.3 Hz, 1H), -2.91 (s, 2H). **^{13}C NMR (101 MHz, DMSO-d$_6$)** δ (ppm): 168.9, 164.3, 141.4, 141.2, 139.82 139.6, 135.5, 134.8, 134.2, 130.2, 128.1, 127.0, 120.2, 120.0, 119.8, 117.5. **HRMS-APCI$^+$** calcd. for $C_{48}H_{34}N_5O_3$ (M+H)$^+$: 728.26; Found: 728.2656.
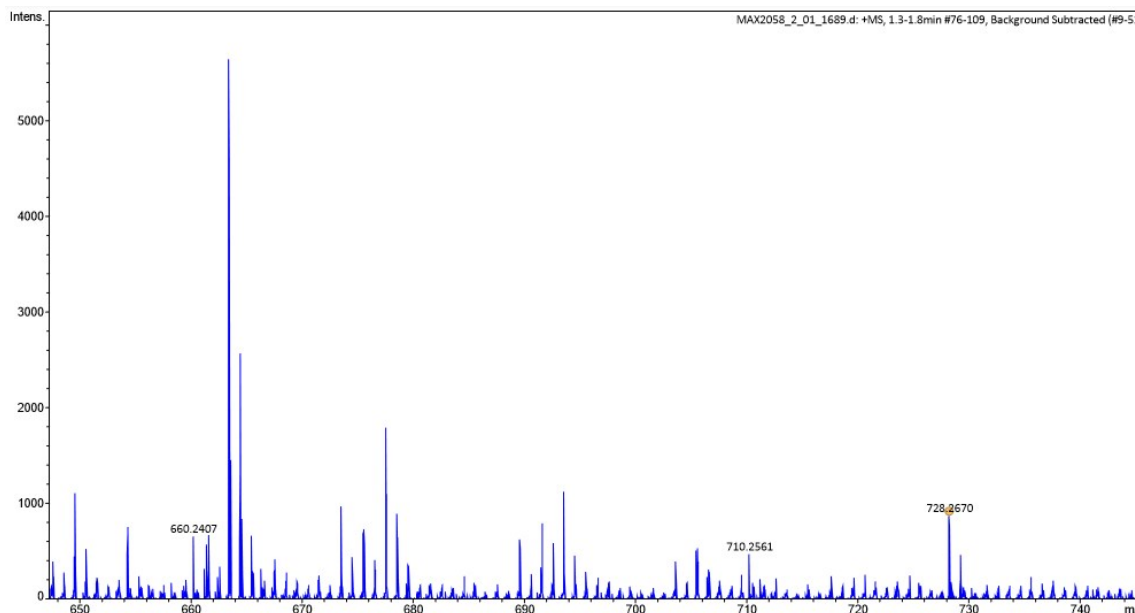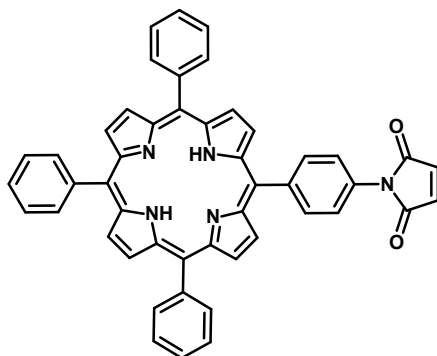
^{1}H NMR (400 MHz, DMSO-d$_6$)

13C NMR (101 MHz, DMSO-d₆)
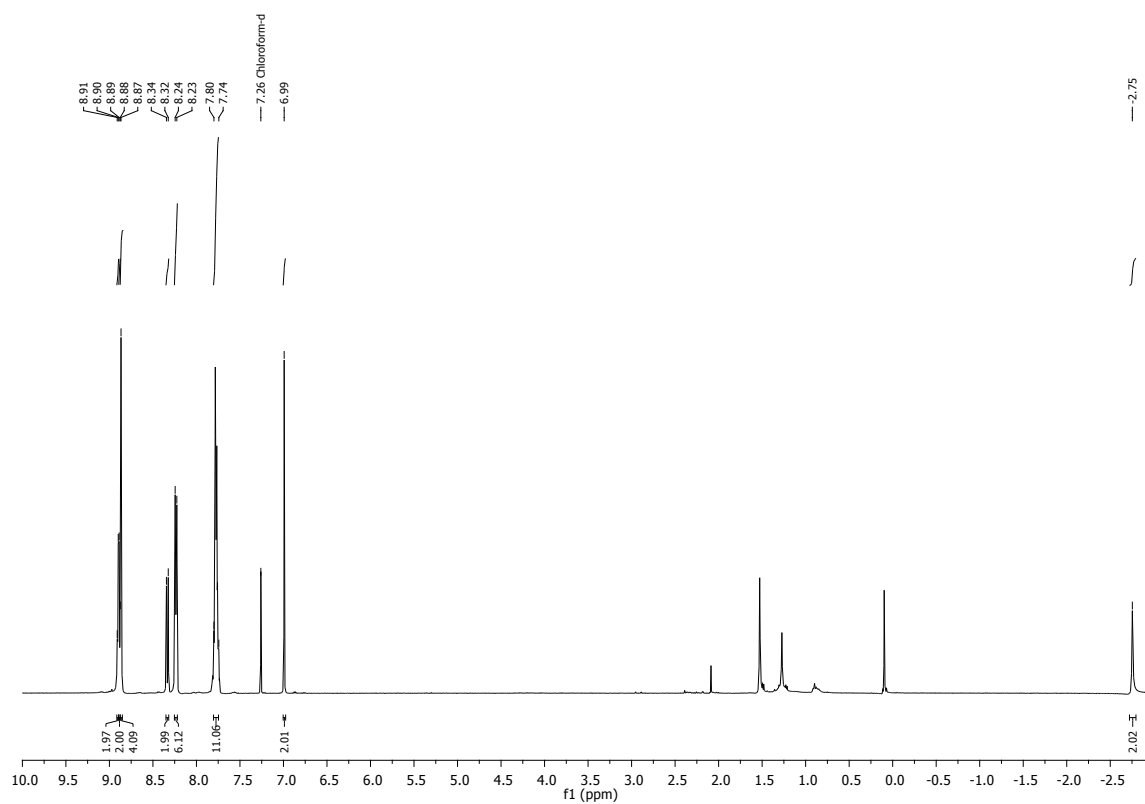

9

HRMS-APCI⁺

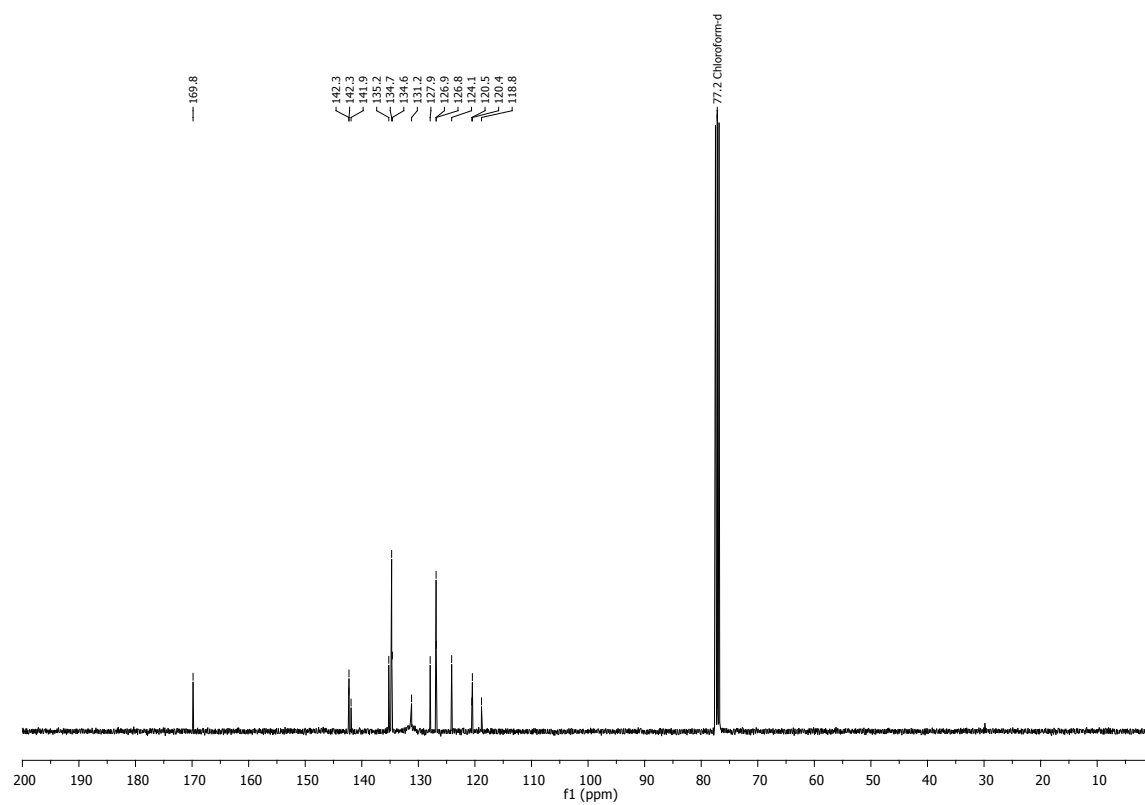**5-(4'-Maleimidophenyl)-10,15,20-triphenylporphyrin (5).** To a stirred solution of 5-[4'-(N-Phenylmaleamic acid)]-10,15,20-triphenylporphyrin (**4**) (2.90 g, 3.97 mmol, 1.00 equiv.) in acetic anhydride (400 mL) was added sodium acetate (0.43 g, 5.20 mmol, 1.30 equiv.). The mixture was stirred for 3 h at 100 ºC in the absence of moisture. After this time, part of the solvent was evaporated under reduced pressure and the reaction extracted with CHCl$_3$/water (1:1). The residue was purified by silica gel chromatography using CHCl$_3$ as eluent to afford the final product as a purple solid; yield: 2.54 g (90%). **¹H NMR (400 MHz, CDCl$_3$)** δ (ppm): 8.90 (d, *J* = 4.8 Hz, 2H), 8.88 (d, *J* = 5.1 Hz, 2H), 8.87 (s, 4H), 8.33 (d, *J* = 8.3 Hz, 2H), 8.24 – 8.22 (m, 6H), 7.80 – 7.74 (m, 11H), 6.99 (s, 2H), -2.75 (s, 2H). **¹³C NMR (101 MHz, CDCl$_3$)** δ (ppm): 169.8, 142.3, 142.3, 141.9, 135.2, 134.7, 134.6, 131.2, 127.9, 126.9, 126.8, 124.1, 120.6, 120.5, 118.8. **HRMS-APCI⁺** calcd. for C$_{48}$H$_{32}$N$_5$O$_2$ (M+H)⁺: 710.2551; Found: 710.2558.

¹H NMR (400 MHz, CDCl₃)

8.91
8.90
8.89
8.88
8.87
8.34
8.32
8.24
8.23
7.80
7.74
7.26 Chloroform-d
6.99
−2.75

1.97
2.00
4.09
1.99
6.12
11.06
2.01
2.02

10.0 9.5 9.0 8.5 8.0 7.5 7.0 6.5 6.0 5.5 5.0 4.5 4.0 3.5 3.0 2.5 2.0 1.5 1.0 0.5 0.0 -0.5 -1.0 -1.5 -2.0 -2.5
f1 (ppm)

¹³C NMR (101 MHz, CDCl₃)

169.8
142.3
142.3
141.9
135.2
134.7
134.6
131.2
127.9
126.9
126.8
124.1
120.5
120.4
118.8
77.2 Chloroform-d

200 190 180 170 160 150 140 130 120 110 100 90 80 70 60 50 40 30 20 10
f1 (ppm)

11

HRMS-APCI⁺
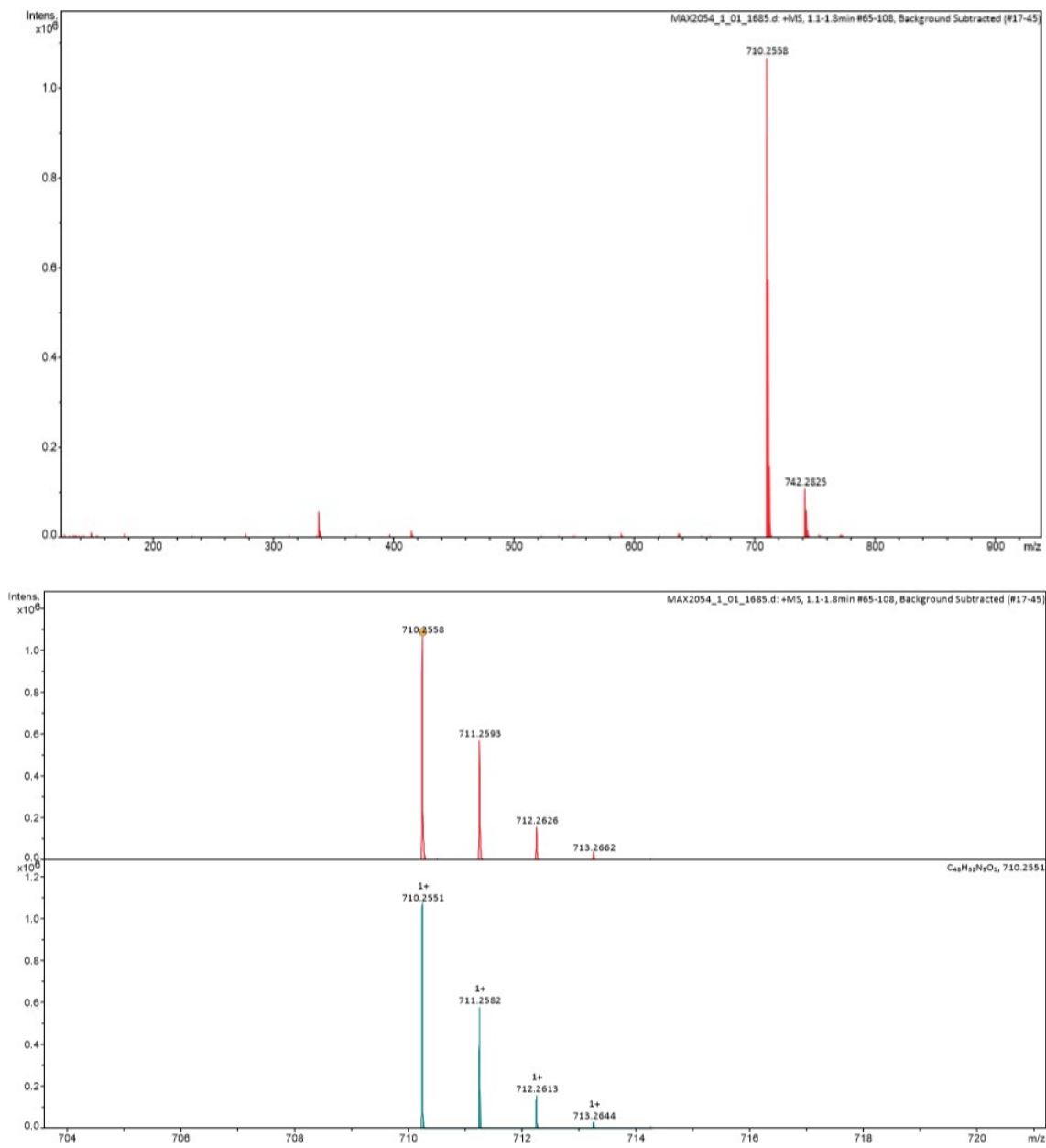
S3. TPP-succ-Fk synthesis

Franckeite was exfoliated by liquid phase exfoliation following the procedure previously described -see main text-.[4]

For each reaction, 10 mL of the obtained exfoliated Franckeite (the approximated concentration is 0.5 mg·mL^{-1} of Fk in iPrOH) are mixed with 25 mg of TPP-mal (100 mg in the case of the *N*-benzyl maleimide) previously dissolved in 10 mL CHCl$_3$. The mixture is sonicated for 5 min and stirred overnight at room temperature. For the cleaning procedure, the suspension was filtered through a polytetrafluoroethylene membrane with a pore size of 0.2 µm, and the solid was washed with CHCl$_3$ several times (around 15 times in this case) to remove excess reagents and physisorbed maleimide.
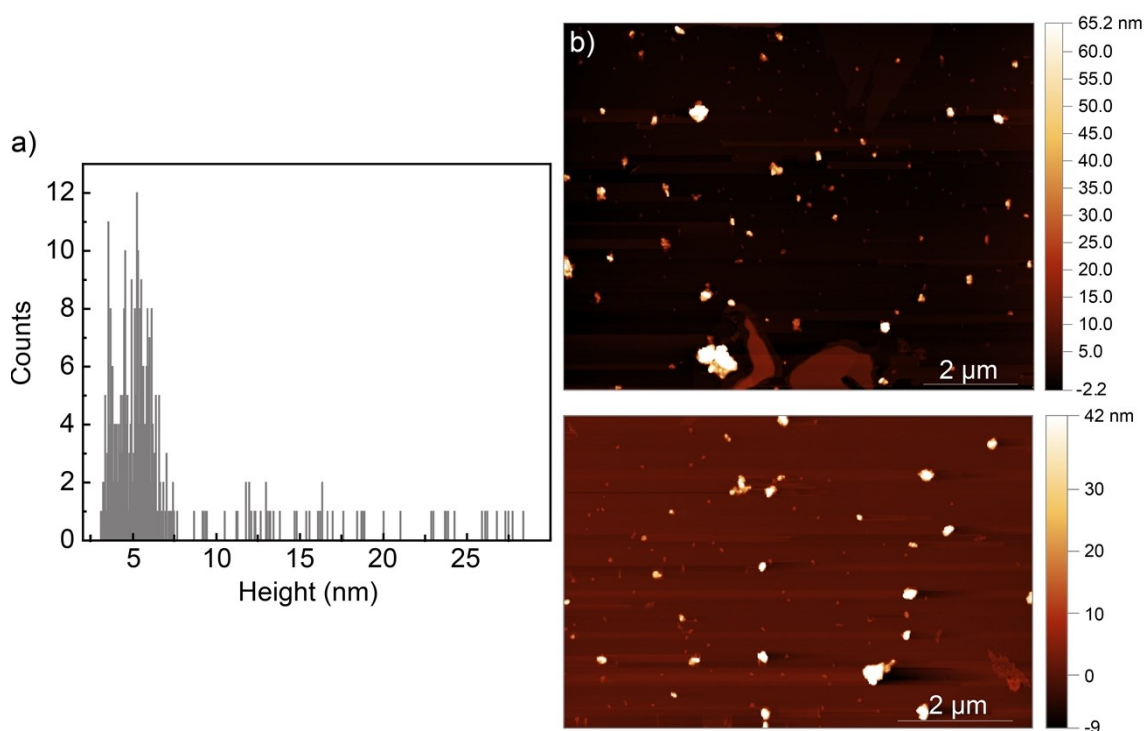
S4. LPE Franckeite

Figure S4. AFM of the colloidal dispersion obtained for the iPrOH-exfoliated franckeite prepared by sonication of a 10 mg·mL^{-1} suspension. a) Statistical analysis of the raw height data. b) AFM micrographs of the sample drop casted and dried over a freshly exfoliated mica substrate.
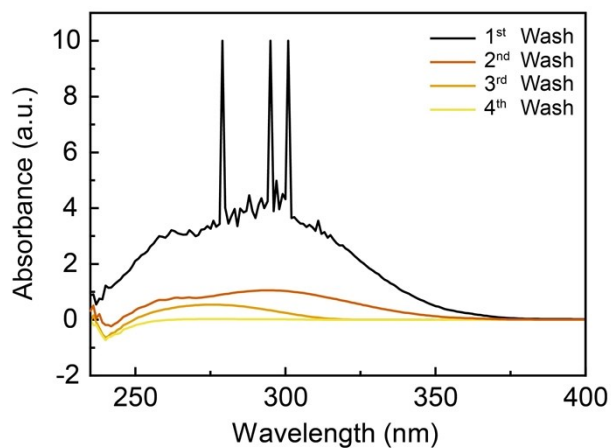
S5. UV-Vis cleaning supernatants

Figure S5. UV-Vis spectra of the supernatants recovered after CHCl$_3$ washing and filtration.
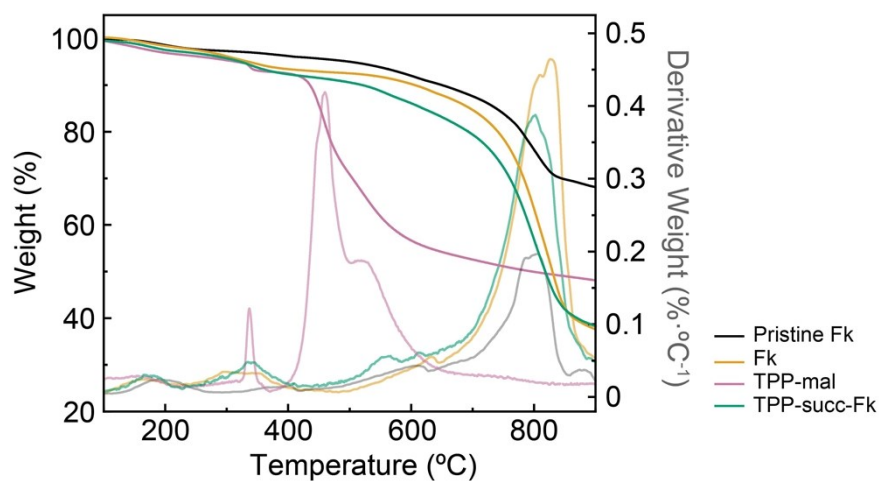
S6. TPP-succ-Fk TGA

Figure S6. TGA (N$_2$, 10 °C·min^{-1}) of pristine exfoliated Fk (black), control Fk (yellow), TPP-maleimide (pink) and functionalized TPP-succ-Fk (green). The first derivatives are shown in thinner lines.
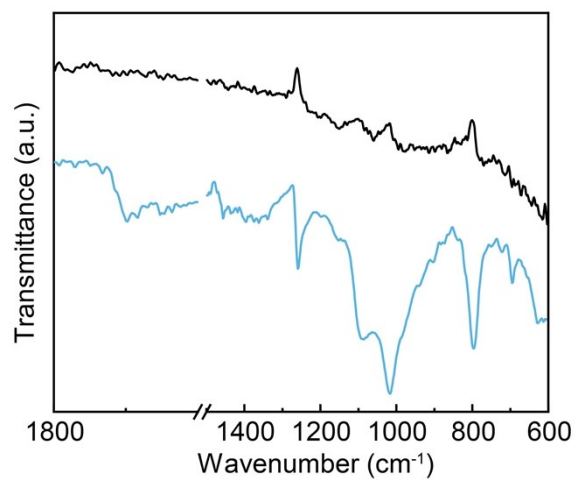
S7. FT-IR of the *N*-benzylsuccinimide-Fk reaction

Figure S7. Comparison of the ATR-IR spectra of Bn-succ-Fk (pale blue) (a) and Bn-succinimide Fk reaction (black) (b).
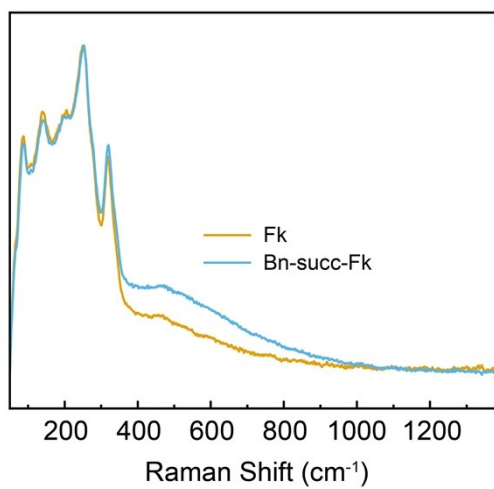
S8. Raman spectra

Figure S8. Raman spectra obtained for the control Fk and the Bn-succ-Fk functionalized sample using a 633 nm laser.

S9. Fk Raman data

Raman shift (cm^{-1})	Phonon mode attribution	Homogeneous material reference			
		Raman shift (cm^{-1})	Compound	State	Literature citation
86	SA	68	PbS	Nanocrystal	[5,6]
	2TA	73		$(PbS)_{1.18}(TiS_2)_2$ misfit	[7]
141	2nd order effect	131	SnS$_2$	Nanosheets	[8]
		135		Nanocrystallites	[9]
		140.5		Bulk	[10]
	TA + TO	151	PbS	$(PbS)_{1.18}(TiS_2)_2$ misfit	[7]
		154		Bulk single crystal	[11]
201	LO(Γ)	203	PbS	$(PbS)_{1.18}(TiS_2)_2$ misfit	[7]
		204		Bulk single crystal	[11]
		215		Nanocrystal	[5,6]
	E$_g$	198	SnS$_2$	Nanocrystallites	[9]
		205		Bulk	[10]
		212		Nanosheets	[8]
		215		Film (CVD)	[12]
253	Combination		PbS + SnS$_2$		[7]
321	A$_{1g}$	309	SnS$_2$	Nanocrystallites	[9]
				Nanosheets	[9]
		312		Film (CVD)	[12]
		315		Bulk	[10]
400-650	2LO(Γ)	412	PbS	$(PbS)_{1.18}(TiS_2)_2$ misfit	[7]
		415		Nanocrystal	[6]
		454		Bulk single crystal	[11]
	3LO(Γ)	630		Nanocrystal	[6]
		632		$(PbS)_{1.18}(TiS_2)_2$ misfit	[7]
	2nd order effect	450-650	SnS$_2$	Nanocrystallites	[9]
				Nanosheets	[8]

Table S9. Interpretation of Raman spectra of powder and exfoliated franckeite

Abbreviations: phonon modes TO: transverse optical; TA: transverse acoustic;

LO: longitudinal optical; SA: spheroidal acoustic. (Γ): Γ point of the Brillouin zone.

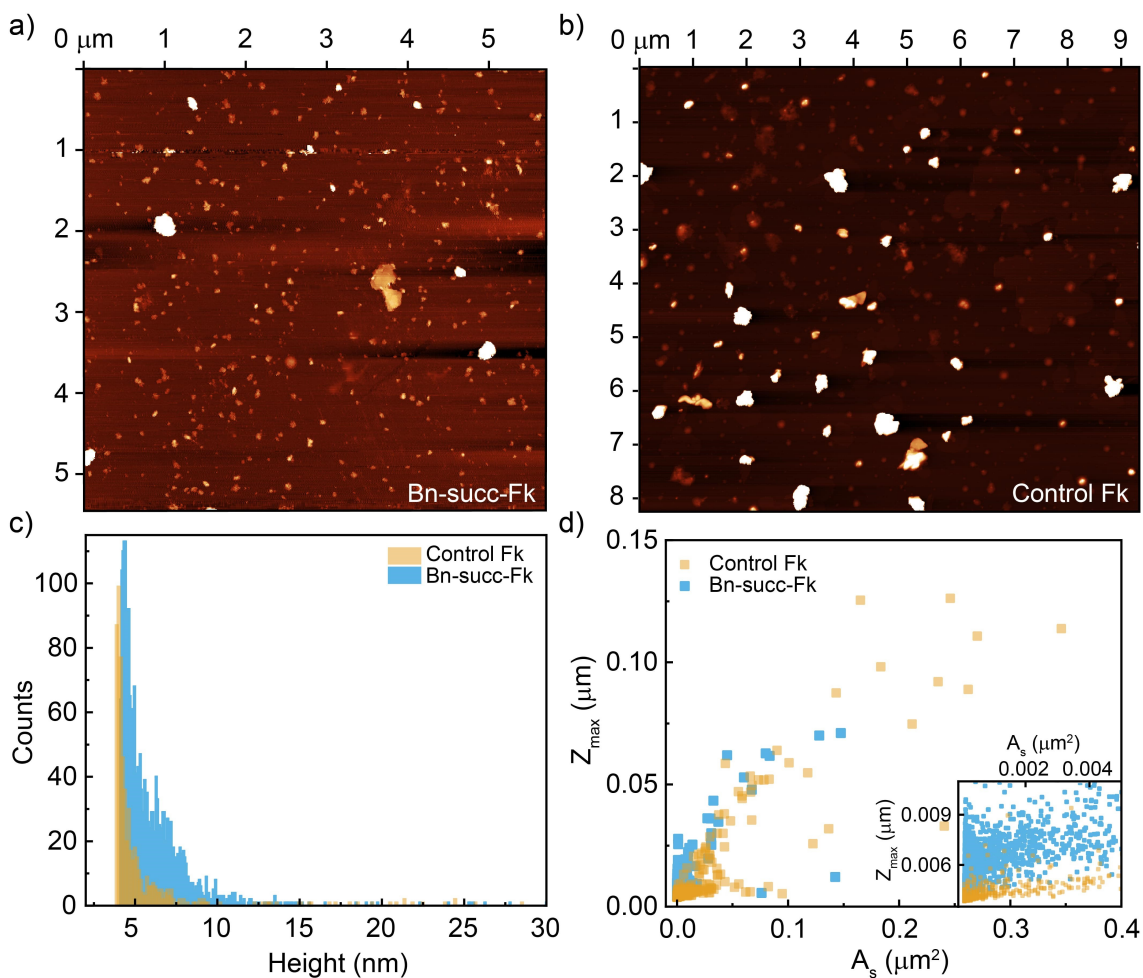# S10. AFM analysis of control and functionalized Fk

Figure S10. AFM micrographs of (a) Bn-succ-Fk and (b) control Fk samples drop casted and dried over a freshly exfoliated mica substrate. c) Statistical analysis of the raw height data obtained for Control Fk (yellow) and Bn-succ-Fk (blue). d) Correlation between base area and mean heights of the individual grains obtained through AFM for Control Fk (yellow squares) and Bn-succ-Fk (blue squares).

The analysis of the AFM obtained for the control Fk and Bn-succ-Fk reveals that no change is performed in the thickness of the unique 2D-2D heterostructure. The majority of flakes are again found under 7.5 nm, meaning 5 or less layer thickness.

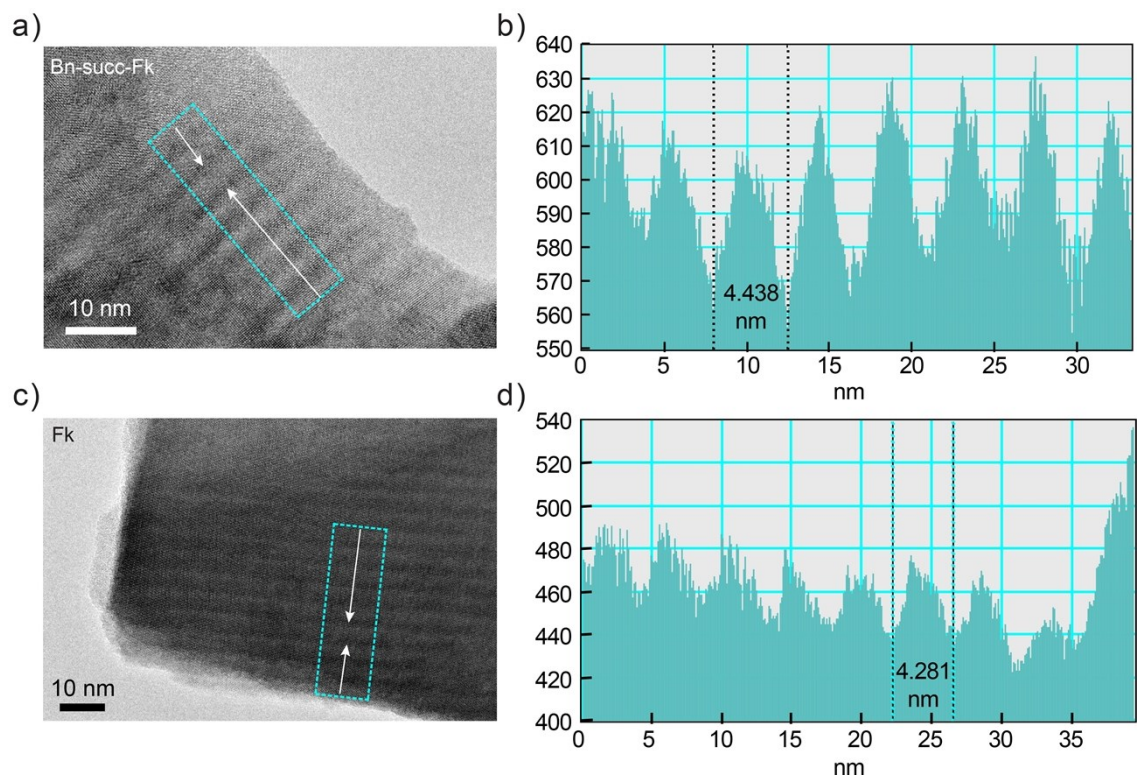## S11. Additional HRTEM measurements

Figure S11-1. [100] HRTEM structure images of (a) Bn-succ-Fk and (c) Fk. b) Intensity profile along the blue square selected in (a), the periodicity corresponds to the one expected for the plane [100] and same happens for Fk (d).
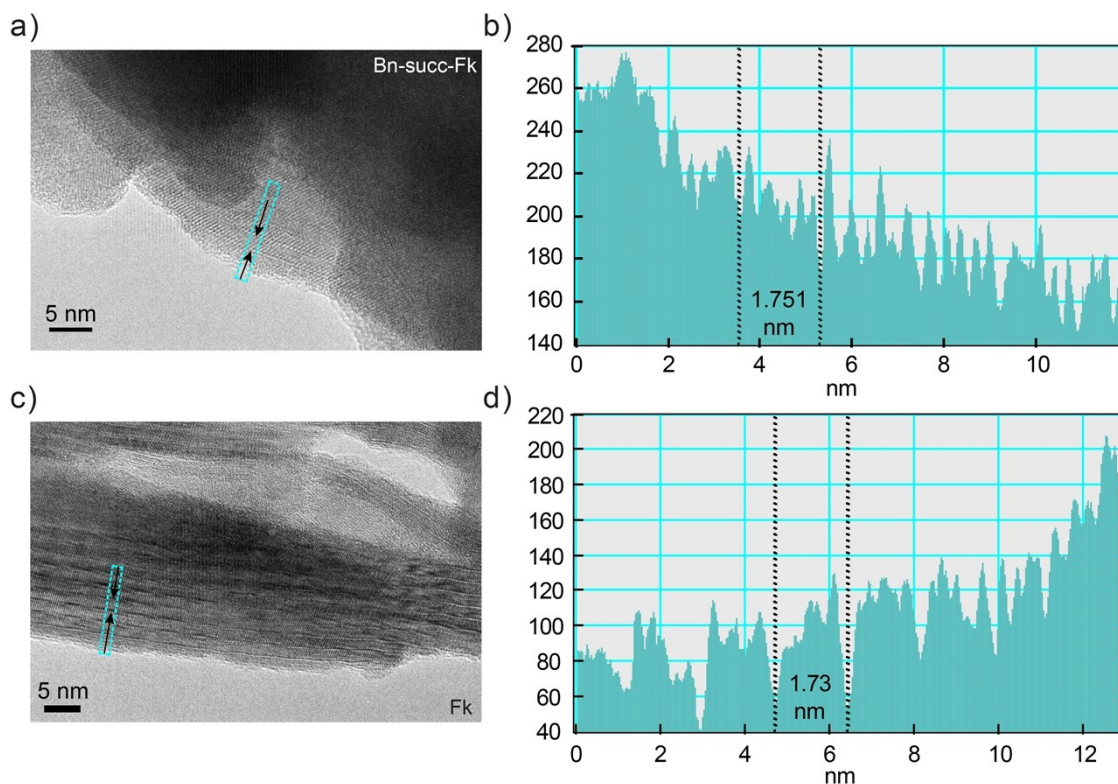
Figure S11-2. [001] HRTEM structure images of (a) Bn-succ-Fk and (c) Fk. b) Intensity profile along the blue square selected in (a), the periodic shade variations can be explained by the [001] projection. The same periodicity is observed for Fk (d).
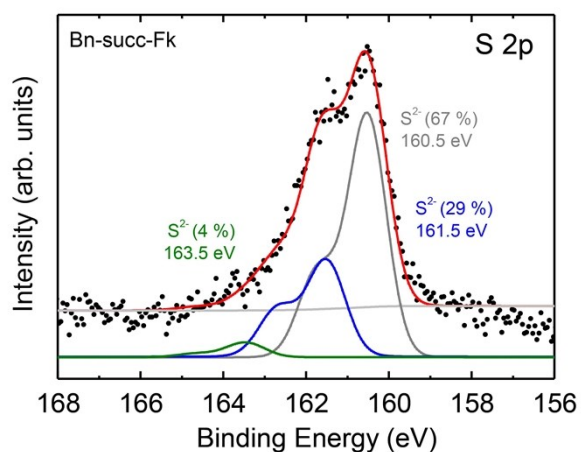
S12. XPS

Figure S12. XPS spectra of S core level for Bn-succ-Fk adding a third component. Although the fitting is improved we do not think it is sufficiently justified.
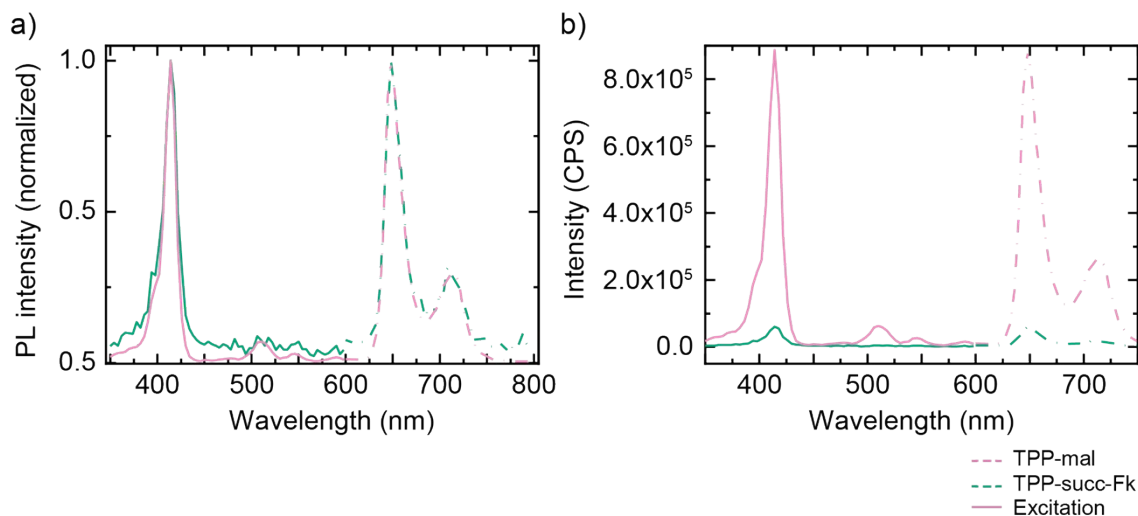
S13. PL and TRPL

a)

b)

- - - TPP-mal
- - - TPP-succ-Fk
—— Excitation

Figure S13-1. a) Normalized excitation (solid line) – emission spectra (dashed line). b) Non-normalized excitation – emission spectra.
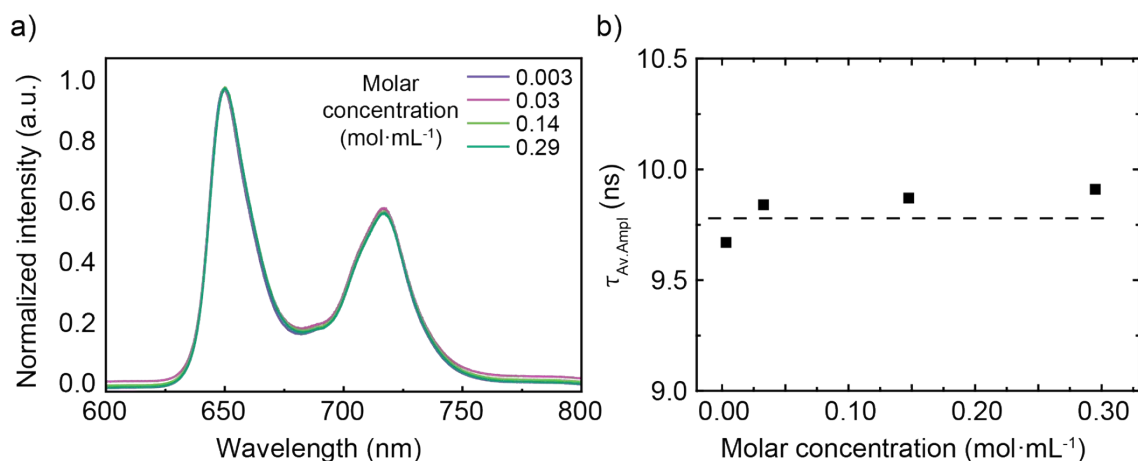
a)

b)

Figure S13-2. a) Normalized photoluminescence spectra and (b) average decay times for different concentrations of TPP-mal dispersions in iPrOH.

Figure S13-2 shows negligible changes in spectra or dynamics for TPP-mal dispersions of different concentrations.

S14. Transient absorption spectroscopy

Transient absorption spectroscopy (TAS) measurements on pristine TPP-mal, Fk and TPP-succ-Fk were performed in order to identify and clarify the interaction between Fk and the functionalizing chromophore. No signal of the TPP-mal in the functionalized sample nor between Fk and TPP-succ-Fk has been observed. This, however, cannot rule out a weak interaction as the sample is functionalized just by a 5-7% and hence the presence of TPP-mal is not detected. The high level of scattering related noise in the measurement might hide small dynamic variations.
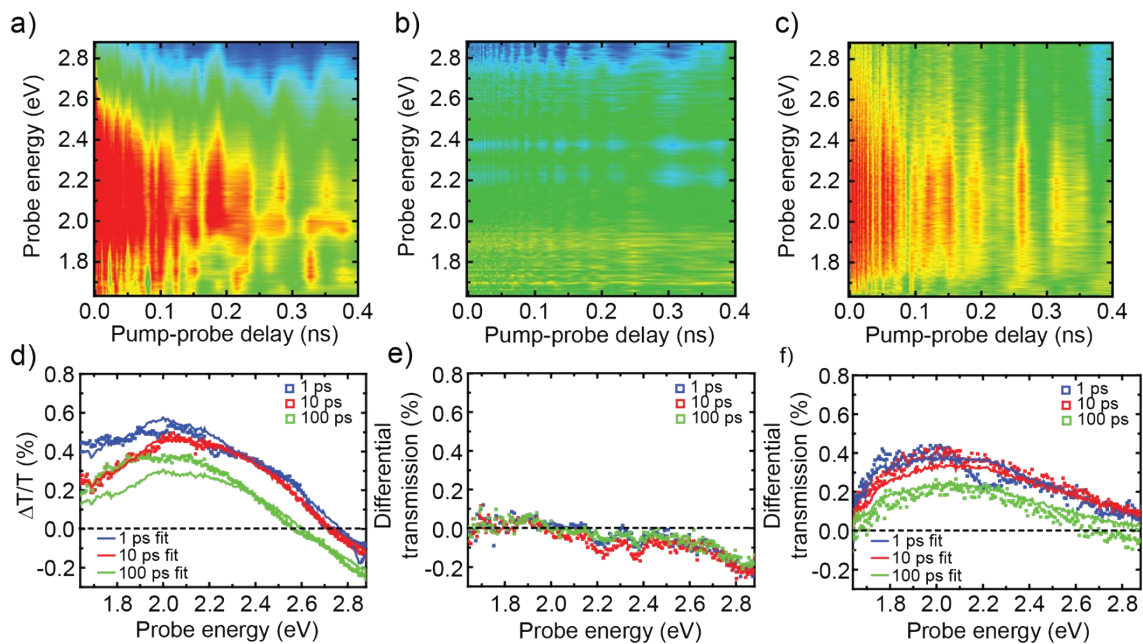
Figure S14-1. Density plot of TAS of Fk (a) TPP-mal (b) and TPP-succ-Fk (c). d), e) and f) are the spectra at different delays of their above plot.
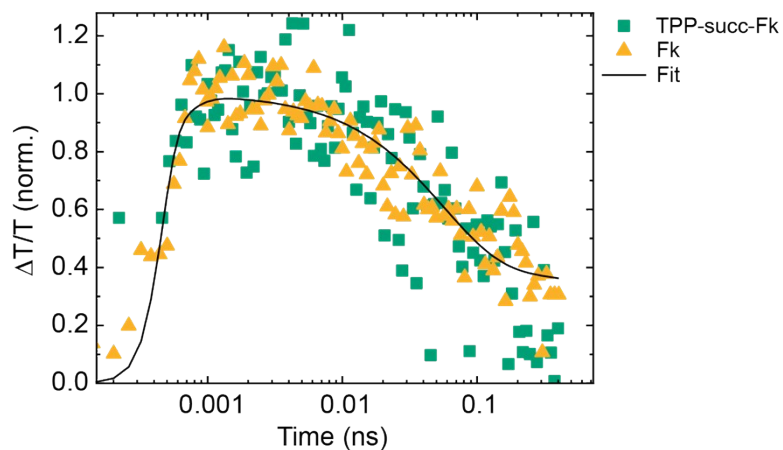

Figure S14-2. Normalized temporal trace of Fk (orange triangles), TPP-succ-Fk (green squares) and the three processes global fit analysis (line).
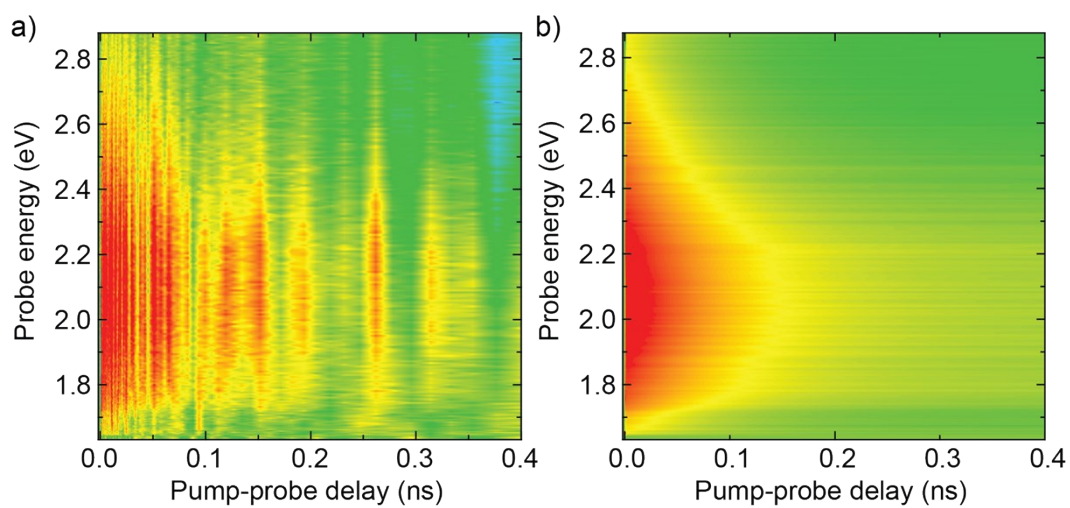
Figure S14-3. TAS density plot measurement of TPP-mal-Fk (a) and its global fit analysis (b).

S15. References

(1) Adler, A. D.; Longo, F. R.; Finarelli, J. D.; Goldmacher, J.; Assour, J.; Korsakoff, L. *The Journal of Organic Chemistry* **1967**, *32*, 476.

(2) Tasan, S.; Licona, C.; Doulain, P.-E.; Michelin, C.; Gros, C. P.; Le Gendre, P.; Harvey, P. D.; Paul, C.; Gaiddon, C.; Bodio, E. *JBIC Journal of Biological Inorganic Chemistry* **2015**, *20*, 143.

(3) Chauhan, S. M. S.; Giri, N. G. *Supramolecular Chemistry* **2008**, *20*, 743.

(4) Molina-Mendoza, A. J.; Giovanelli, E.; Paz, W. S.; Angel Nino, M.; Island, J. O.; Evangeli, C.; Aballe, L.; Foerster, M.; van der Zant, H. S. J.; Rubio-Bollinger, G.; Agrait, N.; Palacios, J. J.; Perez, E. M.; Castellanos-Gomez, A. *Nat. Comm.* **2017**, *8*.

(5) Geim, A. K.; Grigorieva, I. V. *Nature* **2013**, *499*, 419.

(6) Bae, S.; Kim, H.; Lee, Y.; Xu, X.; Park, J.-S.; Zheng, Y.; Balakrishnan, J.; Lei, T.; Ri Kim, H.; Song, Y. I.; Kim, Y.-J.; Kim, K. S.; Özyilmaz, B.; Ahn, J.-H.; Hong, B. H.; Iijima, S. *Nature Nanotechnology* **2010**, *5*, 574.

(7) Yang, W.; Chen, G.; Shi, Z.; Liu, C.-C.; Zhang, L.; Xie, G.; Cheng, M.; Wang, D.; Yang, R.; Shi, D.; Watanabe, K.; Taniguchi, T.; Yao, Y.; Zhang, Y.; Zhang, G. *Nature Materials* **2013**, *12*, 792.

(8) Gong, Y.; Lin, J.; Wang, X.; Shi, G.; Lei, S.; Lin, Z.; Zou, X.; Ye, G.; Vajtai, R.; Yakobson, B. I.; Terrones, H.; Terrones, M.; Tay, Beng K.; Lou, J.; Pantelides, S. T.; Liu, Z.; Zhou, W.; Ajayan, P. M. *Nature Materials* **2014**, *13*, 1135.

(9) Zhang, X.; Meng, F.; Christianson, J. R.; Arroyo-Torres, C.; Lukowski, M. A.; Liang, D.; Schmidt, J. R.; Jin, S. *Nano Lett.* **2014**, *14*, 3047.

(10) Ponomarenko, L. A.; Geim, A. K.; Zhukov, A. A.; Jalil, R.; Morozov, S. V.; Novoselov, K. S.; Grigorieva, I. V.; Hill, E. H.; Cheianov, V. V.; Fal'ko, V. I.; Watanabe, K.; Taniguchi, T.; Gorbachev, R. V. *Nature Physics* **2011**, *7*, 958.

(11) Georgiou, T.; Jalil, R.; Belle, B. D.; Britnell, L.; Gorbachev, R. V.; Morozov, S. V.; Kim, Y.-J.; Gholinia, A.; Haigh, S. J.; Makarovsky, O.; Eaves, L.; Ponomarenko, L. A.; Geim, A. K.; Novoselov, K. S.; Mishchenko, A. *Nature Nanotechnology* **2012**, *8*, 100.

(12) Bertolazzi, S.; Krasnozhon, D.; Kis, A. *ACS Nano* **2013**, *7*, 3246.